Chaos in a CO_2 laser with modulated parameters: Experiments and numerical simulations

Didier Dangoisse, Pierre Glorieux, and Daniel Hennequin
Laboratoire de Spectroscopie Hertzienne, Université des Sciences et Techniques de Lille I, 59655 Villeneuve d'Ascq Cédex, France
(Received 30 March 1987)

A laser with parameters modulated at a frequency f may respond not only at that frequency and its harmonics nf, but also at that of its subharmonics f/n. When the order n of its subharmonics increases indefinitely, the response of the laser becomes irregular, though the system remains deterministic. Many approaches have been used to characterize these different behaviors and the associated attractors, in a CO_2 laser containing an elasto-optic modulator. A quite important similitude has been remarked between the bifurcation diagram of the laser and that of the logistic map $x_{n+1}=1-\mu x_n^2$. More complex chaotic features have also been observed, e.g., generalized bistability between different attractors, and crisis when a chaotic attractor collides with an unstable periodic cycle. The influence of the rate of change of the driving parameters has also been studied. The experimental results show excellent agreement with those provided by the two-level model of the laser.

I. INTRODUCTION

The laser with modulated parameters appears to be not only an excellent device for the investigation of chaotic phenomena but also a useful system for all the applications in which modulated laser radiation is required (e.g., telecommunications, target designation, etc.). From the point of view of applications, the CO_2 laser with modulated losses has long been a subject of interest in connection with intracavity spectroscopy and with the hope to produce giant laser pulses. More particularly, in an attempt to explain the high sensitivity of intracavity laser spectroscopy, Arimondo and Glorieux showed that the laser containing a saturable absorption cell could exhibit damped relaxation oscillations.[1] By modulating the laser at that particular frequency, very strong nonlinear effects can be produced. This excitation of the laser near its resonance frequency or some (sub)harmonics is the basis of the experiments of chaos in this system.

In fact chaos has been observed in modulated CO_2 lasers,[2-7] semiconductor diode lasers,[8] and Nd P_5O_{14} (Ref. 9) nuclear-spin flip[10] and YAG:Nd^{3+} lasers,[11] where YAG represents yttrium aluminum garnet. A wide variety of effects has been observed, some of which are specific to a particular laser system, while some others appear to be general properties of systems exhibiting bifurcations.

The purpose of this paper is to present in a unified way the effects we observed in a modulated CO_2 laser, to characterize them, and possibly to give an efficient modelization together with numerical simulation of the various phenomena which were experimentally observed.

For the last few years, the CO_2 laser with internal modulation has been investigated experimentally and theoretically in the framework of the interest recently developed for chaos and related nonlinear phenomena. Arecchi *et al.* have shown subharmonic bifurcations and generalized bistability in a CO_2 laser containing an electrooptic modulator[2,3] and they measured the dimension of the strange attractor describing the chaotic regime, using the Procaccia-Grassberger method.[4] Midavaine *et al.* observed period-doubling cascades culminating in chaos with periodic windows in a CO_2 laser frequency modulated by an elasto-optic modulator inserted inside the laser cavity[5] and recently Hennequin *et al.* reported the observation of crises in this system.[7] On the theoretical side, Ivanov *et al.* predicted chaos in a solid-state laser with periodically modulated losses,[12] and recently Erneux *et al.* calculated the influence of the modulation frequency in this kind of laser, showing a new set of bifurcations.[13] Multistability has also been predicted by Matorin *et al.*[14]

In Sec. II we present the waveguide CO_2 laser, the elasto-optic modulator, and the signal processing techniques which have been used throughout the experiments. The direct observation of the period-doubling cascade as measured on the intensity delivered by the laser is described in Sec. III. Digital recording of the signal allows one to compare their time development and, by choosing similar sequences, to exhibit the sensitivity to initial conditions of the system. It is also possible to reconstruct the strange attractor from these time series. Such reconstructions are presented in Sec. IV together with other on-line observations at fixed parameters, e.g., statistical analysis of the distribution of points in Poincaré sections of the reconstructed attractor. Periodic sampling of the signal at the same frequency as that of the external modulation allows one to visualize directly on an oscilloscope the bifurcation diagrams of the laser with modulated losses or frequency. The bifurcation diagrams obtained using the modulation amplitude or the laser detuning as control parameters are given in Sec. V. This approach using bifurcation diagrams proved very useful in assigning various phenomena observed in the chaotic region and which are presented in the following sections.

A two-level model of the laser using adiabatic elimination of the polarization appears to describe quite accurately the modulation characteristics of the CO_2 laser with modulated losses or frequency. Extensive numerical simulations have been made on the basis of this model and helped in understanding and clarifying some effects observed on the laser output. The following sections are devoted to these effects, namely, "generalized bistability," crises, and dynamical deformation of bifurcation diagrams. In Sec. VII we show that our laser system may be characterized by several attractors for one set of operating conditions. Depending on the initial conditions, the system evolves towards one attractor or another and exhibits hysteresis. Both the experimental setup and the numerical model exhibit different kinds of crises, i.e., abrupt changes in the qualitative properties of an attractor as shown in Sec. VIII. In Sec. IX a brief discussion of the effects related to the dynamical deformation of the bifurcation diagram is given.

II. EXPERIMENTAL SETUP

The experimental setup consists essentially of a sealed-off waveguide CO_2 laser in the cavity of which an elasto-optic modulator is inserted. The laser cavity is 25 cm long and a dc discharge runs 4 mA through 7 kV typically. The 19-cm-long active medium is composed of a mixture of CO_2, CO, Xe, and He at a pressure of 50 Torr inside a 2-mm-bore alumina tube closed by antireflection-coated windows. The laser power is coupled out through a 90% reflecting mirror and also via specular reflection on the grating. It reaches 300 mW typically and the signal-to-noise ratio is in excess of 60 dB. The mode width depends on gain and pressure inside the cavity medium. It varies from 200 MHz to the free spectral range of the cavity (500 MHz) depending on operating conditions. The cavity length and thus the laser frequency are adjusted by applying a voltage to the piezoelectric ceramic which holds the end mirror.

The elasto-optic modulator is made of a ZnSe crystal squeezed by a stack of piezoelectric ceramics fed by a high stability programmable synthesizer. The stress due to these ceramics induces birefringence in the crystal in a way similar to the electro-optic effect.[15] In fact, the motion of the ceramics changes the laser output through two phenomena: (i) The reflecting power of the grating depends on the polarization of the incoming beam and the orientation of the grating fixes the polarization direction of the laser beam, and thus the modulation of the optical axes of the crystal induces a loss modulation; and (ii) the length of the crystal and consequently the optical length of the cavity are changed when the crystal is pressed and thus the layer may be frequency modulated.

The relative efficiency of these modulations depends on the frequency of the voltage applied to the ceramics which press on the crystal. Depending on this frequency, various mechanical vibration modes of the crystal can be excited. It is possible to select either amplitude (AM) or frequency (FM) modulation for the laser by correctly choosing the vibration mode of the elasto-optic crystal. When a modulation frequency of 330 KHz is used, a 100 mV voltage applied to the ceramics stack produces a frequency shift of 1.8 MHz which corresponds to a change of the optical length of the cavity of 19 nm, while the same voltage induces a 0.5% loss modulation via stress-induced birefringence. These modulation rates are strongly dependent on the modulation frequency because of the vibration modes of the crystal. Moreover, as the laser dynamics present some resonance frequencies, the efficiency of these modulations strongly varies with their frequency.

The laser intensity is monitored by an HgCdTe photovoltaic detector and stored in a digital oscilloscope in series of 1024 samples of 8 bits. The intensity spectrum of the laser may be measured with an Advantest TR 4131 E spectrum analyzer. Both systems are connected to a microcomputer for further data processing. In the purpose of monitoring the changes in the attractors, the laser intensity and its time derivative obtained by analog differentiation can also be visualized on an oscilloscope used in the X-Y mode.

III. DIRECT OBSERVATION OF THE SIGNALS

Various quantities may be used as control parameters. The most commonly used in our experiments are the modulation amplitude and the laser detuning.

In this section we shall describe the evolution of the laser output as the modulation amplitude V is increased, with an elasto-optic modulator working in the frequency modulation mode. Similar results have been obtained when the modulation is operated in the AM mode. This evolution is illustrated on Fig. 1. We start from a situation in which the laser is oscillating cw in the absence of modulation ($V=0$). At low modulation [Fig. 1(a)] the laser response is linear and the output intensity is sinusoidally modulated. When V is increased, the output period suddenly doubles; then if V is further increased [Fig. 1(b)], the modulation on the laser output is larger; then a new bifurcation occurs, where a $4T$ component appears [Fig. 1(c)]. For a very little increase of the modulation, a $8T$ component appears [Fig. 1(d)]. At slightly larger modulation amplitudes, any regularity in the laser intensity is lost; it appears first as a $4T$ "noisy" signal, then a $2T$ "noisy" signal where the maxima of this signal lay in two bands which eventually melt into a single band and the maxima may have any value in this band. In this situation the signal appears as a noisy T-periodic sine wave. At higher modulation rates, the chaotic behavior still evolves and disappears when V still increases. At this point, the output intensity is $3T$, then $6T$ periodic, before returning to a chaotic regime. Other periodic behaviors, e.g., $5T$, may appear at higher modulation rates but there the system is mostly chaotic with a "noisy" $3T$ behavior.

Such a scenario of a period-doubling cascade leading to chaos and periodic regimes was also observed by Arecchi *et al.* in a CO_2 laser with loss modulation using an intracavity electro-optic modulator.[2] The period-doubling cascade and the inverse cascade may be considered as an experimental indication that the irregular part of the evolution, i.e., that illustrated from (e) to (g)

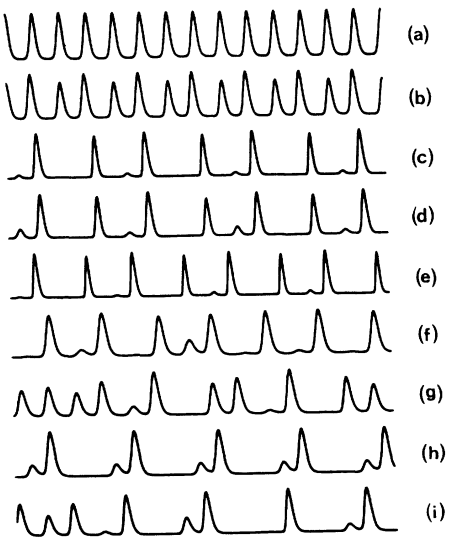

FIG. 1. Time evolution of the laser output intensity as the modulation amplitude increases: (a) T, (b) $2T$, (c) $4T$, (d) $8T$, (e) "noisy $4T$" beginning of the inverse cascade, (f) middle of inverse cascade, "noisy $2T$," (g) first fully chaotic regime, (h) $3T$, (i) "noisy $3T$" regime.

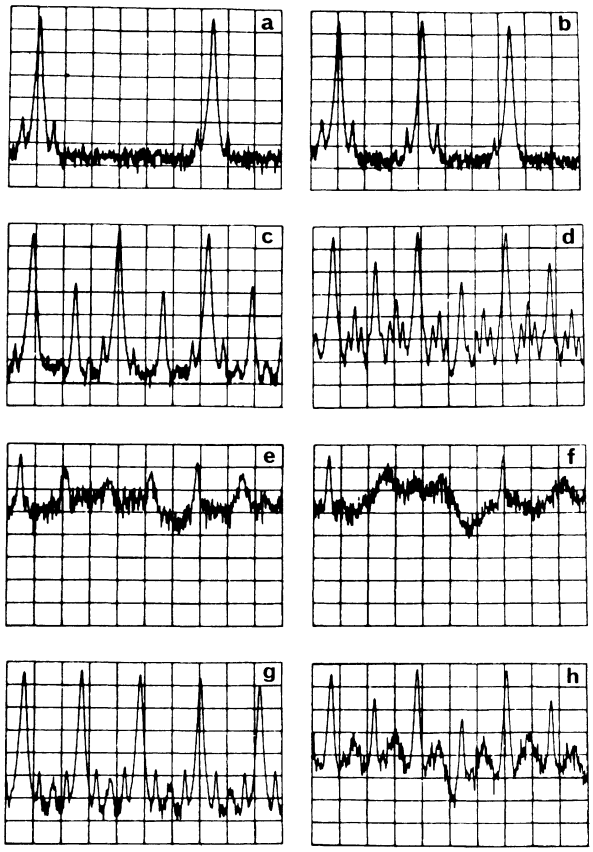

FIG. 2. Spectral analysis of the laser intensity. Modulation frequency: 330 kHz. Span: 50 kHz per division. Weak sidebands at 25 kHz are due to the laser supply. (a) T-periodic regime, (b) $2T$, (c) $4T$, (d) $8T$, (e) and (f) inverse cascade $4C$ and $2C$, (g) $3T$ regime, and (h) chaos.

on Fig. 1, is due to deterministic chaos.[16–18]

To identify the spectral content of the signals corresponding to the different driving voltages V applied to the modulator, the output of the spectrum analyzer corresponding to increasing values of V has been plotted. Examples of these spectra are shown on Fig. 2 which clearly exhibits the successive onset of the various subharmonics of the cascade discussed above: Only the frequency f is visible, then $f/2$, $f/4$, $f/8$. When this cascade converges, a broad background suddenly appears but some peaks at the subharmonic frequency temporarily remain above the continuous spectrum at modulation values corresponding to the inverse cascade. In the $3T$-periodic regime, peaks at frequency $f/3$, then $f/6$, are clearly seen. In a chaotic regime, a spectrum with a broad peak is often observed at frequencies $f/2$, $f/3$, or $f/5$ depending on the modulation amplitude. This evolution inside the chaos will be confirmed by further measurements using other techniques.

Generally speaking, the values of the driving voltage V at the bifurcation points are functions of the laser cavity detuning and consequently of the laser frequency. Figure 3 reports the values of V corresponding to the various bifurcations versus the voltage V_{PZT} applied to the piezoelectric element which tunes the laser cavity length. The diagram is the wider at the top of the laser mode profile ($V_{PZT}=500$ V) but the phenomenology is richer for a cavity about half detuned ($V_{PZT}=250$ V) where the higher-order regimes in the chaos were observed. Generalized bistability has also been observed in that region and will be discussed further in Sec. VIII. Also note that there is a reversal of this tendency when the laser is operated at a frequency near the edge of its emission mode. The asymmetry of the diagram is simply due to the nonlinearity of the ceramic used to tune the laser. Such diagrams depend indeed on the laser gain, a parameter whose influence was not systematically investigated here. In most conditions, the detuning just acts as a reduction of the gain. This is in agreement with the properties of Eq. (5) presented in Sec. II.

Recording of a large series of signals allows one to visualize the sensitivity to initial conditions of the trajectories in the chaotic regime. This may be done by selecting those trajectories which have very similar behaviors. Figure 4 shows such sequences in which the trajectories are identical within the accuracy of the analog to digital converter, for several periods of modulation. These trajectories are shown to eventually diverge and the difference between nearby trajectories is exponentially growing in the first times. The divergence rate K may be evaluated from such trajectories using the same method as Derstine *et al.*[9] In the region of chaos just following the accumulation point of the period-doubling cascade, K has been estimated as 50 kHz. This value may be considered as an evaluation of the largest positive Lyapounov exponent since, as the CO_2 laser with modulated parameters is a low-dimensional system, it is

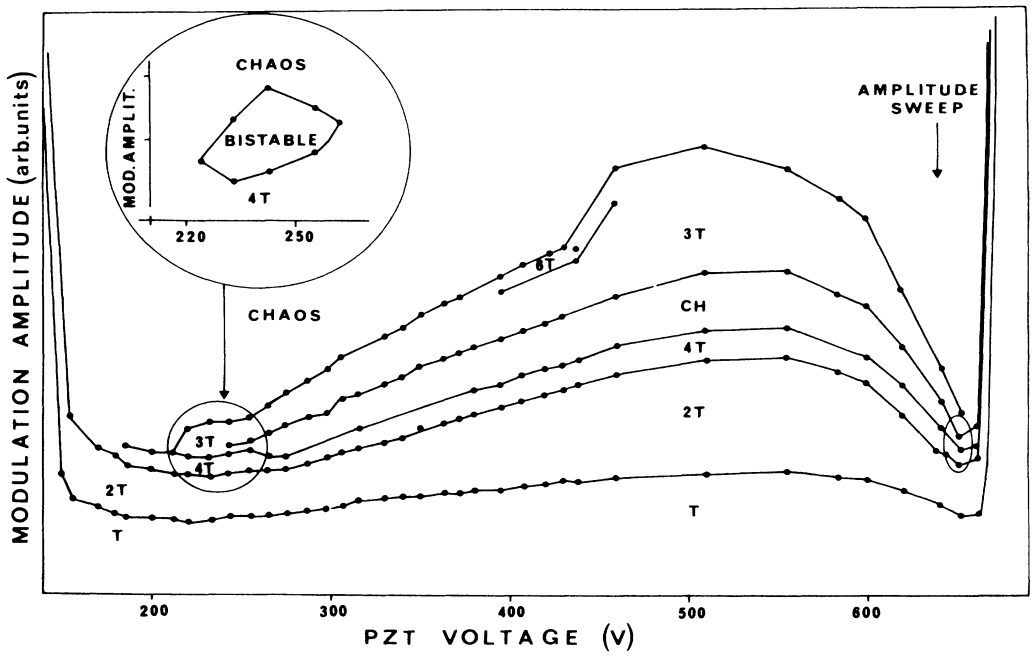

FIG. 3. Dependence of the bifurcation points vs the laser cavity detuning indicated by the PZT voltage. The asymmetry is due to the nonlinearity of the PZT. Generalized bistability is observed in the circled regions.

reasonable to conjecture that each variable reflects rather faithfully the characteristics of the attractor.[18,20] It is in agreement with the measurement of the correlation entropy reported in Refs. 4 and 6.

IV. RECONSTRUCTION OF THE ATTRACTORS. STATISTICAL ANALYSIS

It is not possible to measure the values of all the variables in our experimental system and thus the attractors cannot be reconstructed in the phase space of the variables. However, time series of a single measured quantity $X(t)$ allow the rebuilding, in a new phase space, of trajectories which are topologically identical to those in the original phase space. For instance, it is possible to draw a representation of the attractor using as representation space either $X(t)$, $X(t+\tau)$, $X(t+2\tau)$, ... or $X(t)$ and its successive derivatives $\dot{X}(t)$, $\ddot{X}(t)$, ..., where X is one of the variables of the flow and τ is an arbitrary time.

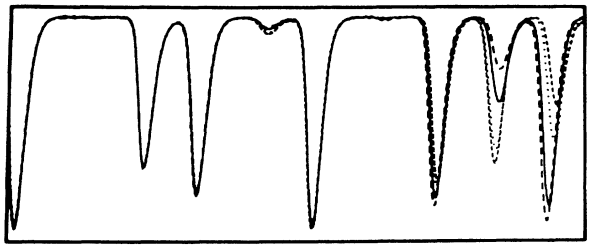

FIG. 4. Sensitivity to initial conditions in the laser with modulated parameters. Four different trajectories corresponding to nearly initial conditions have been plotted with different lines for a time duration of about 30 μs.

The latter method was used extensively during the experiments in a slightly modified version. Only a projection of the reconstructed attractor was visualized by monitoring the output intensity and its time derivative on an X-Y oscilloscope. Unfortunately the access to the second derivative is not easy because of the strong signal attenuation in simple analog differentiating circuits. Consequently, the results of the reconstruction via the time derivatives will not be reported here. However, this method, which allows on-line monitoring of the attractor evolution, appeared extremely useful for the observation of the crises as reported in Sec. VIII.

The reconstruction via successive values of $I(t)$ is very easy to carry out with almost immediate processing of the datas because of the direct access to the variables. The time τ between the different terms of the time series is obviously a multiple of the sampling time Δt of the digital oscilloscope. In the results presented below, it was empirically chosen in order to reflect the most clearly the dynamics of the system. Practically, a value of $12\Delta t$, which is about one-fifth of the modulation period, gives the best results. Series of 25×1024 points were recorded for five different values of the modulation amplitude in the region of chaotic behavior as indicated in Fig. 5. All the diagrams were normalized to the maximum intensity in the displayed series. The shape of the attractor reconstructed from the experimental datas indicates that the system is certainly low dimensional because the trajectories already do not cross in a three-dimensional pseudo phase space. The stratification property is clearly seen in all diagrams as is usual for strange attractors. Moreover, the similarity between the attractors before and after the $3T$-periodic regime [Figs. 5(b) and (e), respectively] indicates that there exists some continuity in the characteristics of the attractor on both sides of the $3T$

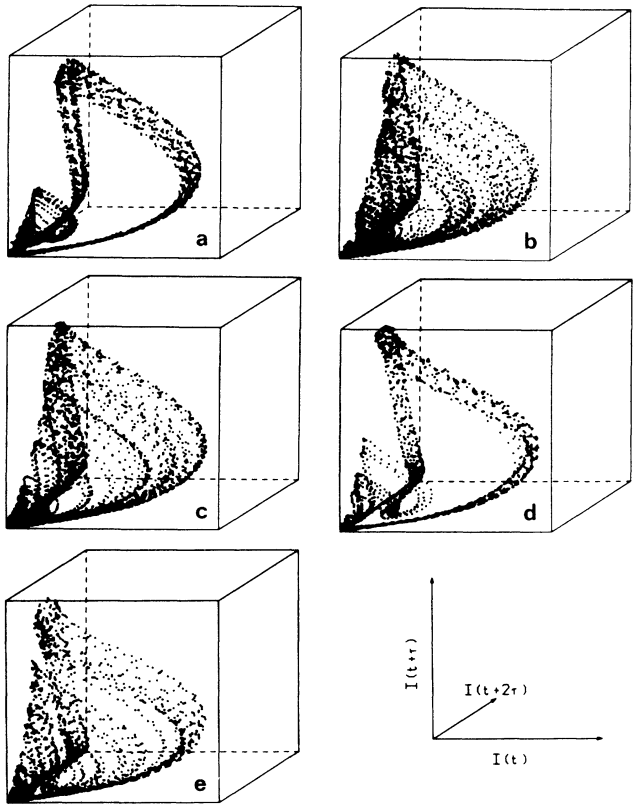

FIG. 5. Reconstruction of the attractor from a time series of the laser intensity $I(t)$, $I(t+\tau)$, $I(t+2\tau)$. The scales have been normalized in each case. (a) Just above the accumulation point, (b) in the middle of the first chaotic region, (c) just before and (d) after the $3T$ region, (e) in the second chaotic region.

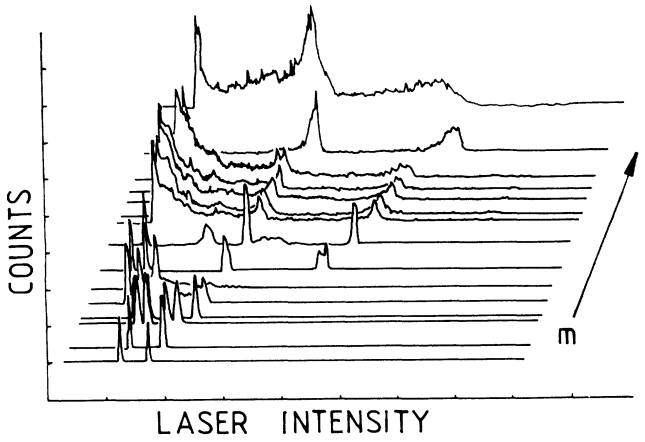

FIG. 6. Statistical analysis of the sampled laser intensity for various values of the modulation amplitude. All scales in arbitrary units.

regime. This point may be surprising since, as will be seen in Sec. V, the $3T$ regime is not the periodic window associated with deterministic chaos following a period-doubling cascade. Note also that in Fig. 5(d) the attractor explores three regions of the phase space as in the inverse cascade situation.

Even if such diagrams do not provide quantitative information on the chaotic behavior, they give us additional evidence that the irregular behavior of the laser is not due to noise. In fact Poincaré sections of these diagrams are much easier to describe and may also provide insight into the properties of the different regimes exhibited by the laser with internal modulation. These sections will not be discussed here since the same information may be gained from the bifurcation diagrams which will be presented in Sec. V. Before going into this approach, it is interesting to present the result of a statistical analysis of chaos. In that purpose, the laser output intensity is periodically sampled and histograms of these samples have been drawn for different values of the modulation amplitude from the first period-doubling bifurcation to chaos well above $3T$-periodic region. The histograms shown in Fig. 6 exhibit the main features of the period-doubling cascade, i.e., the appearance of a wide distribution following period-$2T$ and period-$4T$ bifurcations. The statistics inside chaos have some similarity with these obtained by Farmer in the case of the logistic map,[21] namely, a bounded distribution with sharp asymmetric peaks: Starting from the lower (upper) limit towards the center of the intensity range, every maximum in the histogram appears as a discontinuity and is followed by a slow decrease of the probability distribution. Boundary crises in which the attractor suddenly expands may also be seen in the middle of the explored range of m values.

V. BIFURCATION DIAGRAMS

The observation of bifurcation diagrams (BD's) provides the most convenient tool to investigate the influence of various control parameters on a chaotic system. Such diagrams are easily obtained in our experiments using a stroboscopic method. A sample and hold module is synchronized on the modulation signal and stores a signal proportional to the laser output intensity at some definite time of the modulation sine wave. As it is synchronized on the modulation, if the response of the system is T periodic, the sampler delivers a single-valued output. In case of nT-periodic response, n different values are successively available at the sampler output. When the laser is chaotic, any periodicity in the sampler output is lost and series of apparently random values, which reflect the statistics of chaos, are obtained.

In fact, this stroboscopic picture is quite equivalent to a projection of a Poincaré section in the phase space associated with the intensity I, the population inversion D, and the phase modulation ϕ. The periodic sampling restricts the points considered to those corresponding to a well-defined value of ϕ. As the population difference D is not experimentally measurable, the BD's are shown in a two-dimensional picture where the values of the sampled intensity only are displayed versus the control parameter. These plane representations of the system evo-

lution appear quite convenient to describe the evolution of the attractors with the laser cavity length or the modulation amplitude as control parameters.

A. Bifurcation diagrams versus modulation amplitude

When the voltage applied to the elasto-optic modulator is used as a control parameter, one BD summarizes a set of recordings of the time development of the laser output intensity such as that presented on Fig. 1. A typical BD is shown on Fig. 7 for increasing values of the modulation. At very low modulations, the system is approximately linear and responds at the same period as that of the excitation T. Above some threshold indicated as V_1 on Fig. 7, the response is also periodic but at $2T$, i.e., twice the modulation period. A new bifurcation is observed for $V=V_2$ and the BD is then made of four branches but the two lower amplitude branches can hardly be distinguished because of the particular sampling time chosen for this experiment. The $8T$ response is just visible. Then the system enters the chaotic regime at V_3; this appears as a "broadening" of the branches of the BD. After a small increase of V, the whole domain between zero and the maximum intensity is explored (V_4). As V is further increased to V_5, the chaos suddenly disappears and a $3T$-periodic regime appears, two branches of which overlap near zero. The next bifurcation leads to a $6T$ response and then to chaos again.

This bifurcation diagram presents strong similarities with that of the logistic map[16–18] and the comparison between them can be done on three properties: the harmonic cascade, the inverse cascade, and the universal sequence.

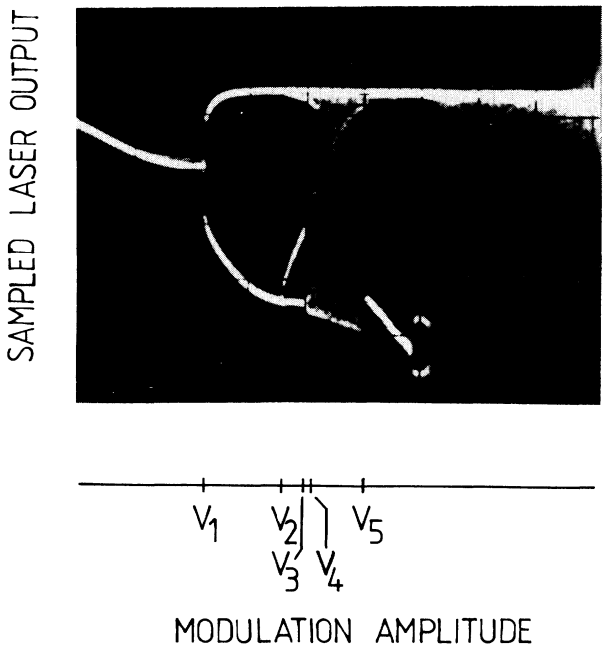

FIG. 7. Bifurcation diagram with the modulation amplitude as a control parameter.

Concerning the period-doubling cascade, the two BD's behave in a similar way; the bifurcations occur on decreasing ranges with ratios of the same magnitude. However, the $8T$ domain, which appears clearly on the logistic map BD, almost disappears in the experimental BD. This may be due to the noise which scrambles the regimes of high subharmonic order as shown in Ref. 22. Note also that the width of the subharmonic zones of the logistic map decreases asymptotically in a geometric progression of ratio 4.7. The width of the $8T$ region is thus expected to be about 100 times smaller than that of the T-periodic regime. The inverse cascades also are similar in the two BD's. In the chaotic regime, the laser system samples a wider and wider region, going through the noisy $8T$, $4T$, and $2T$ regimes as the logistic mapping does. The statistics of the sampled points inside the fully chaotic region follow tendency laws similar to those of the corresponding part in the BD of the logistic map.

However, this similarity disappears as long as the universal sequence is concerned. The $3T$ regime is the only "window" which is clearly visible on the BD, although $5T$ regimes were also observed. As is suggested by the evolution of this "window" with laser cavity detuning, this regime is not that associated with the $3T$ window of the scenario of transition to chaos through the period-doubling cascade[16] but it is rather due to another attractor whose basin of attraction evolves with the laser cavity detuning. Two points confirm the assignment of the $3T$ behavior to a new attractor instead of to the periodic window inside a chaotic region: (i) Its width may be as large as that of the $2T$ regime while in the logistic mapping, it is about 100 times narrower, and (ii) there is a discontinuity between the sampled values in the $3T$ regime and the maxima in the statistics of the chaotic samples while in the logistic map and similar systems, the $3T$ values correspond to the strongest peaks in that distribution. It is then likely that at least two attractors may exist in the laser with modulated parameters. Depending on the laser operating conditions, they may coexist or compete and these processes give rise to generalized bistability and crises (see Secs. VII and VIII).

B. Bifurcation diagrams versus laser frequency

New types of BD's may be observed using the laser frequency as control parameter while the modulation amplitude is kept fixed. A whole family of new BD's is obtained and the two following examples provide an overview of the interests and limits of this approach.

In the first BD [Fig. 8(a)] a large modulation amplitude was used and the cavity length is swept on about one mode spacing ($\Delta l \simeq 5\ \mu$m) by varying the voltage applied to the PZT which holds the end mirror. In the operating conditions of Fig. 8, the gain is relatively weak and the output power drops to zero in the far wings of the mode. The corresponding BD exhibits a complete sequency of bifurcations. Starting from high voltages, the following bifurcations are successively encountered: first a period-doubling bifurcation and chaos, then a $3T$ regime and a new chaotic zone, and, later, the same sequence in inverse order: $3T$, chaos, $4T$, $2T$, and eventu-

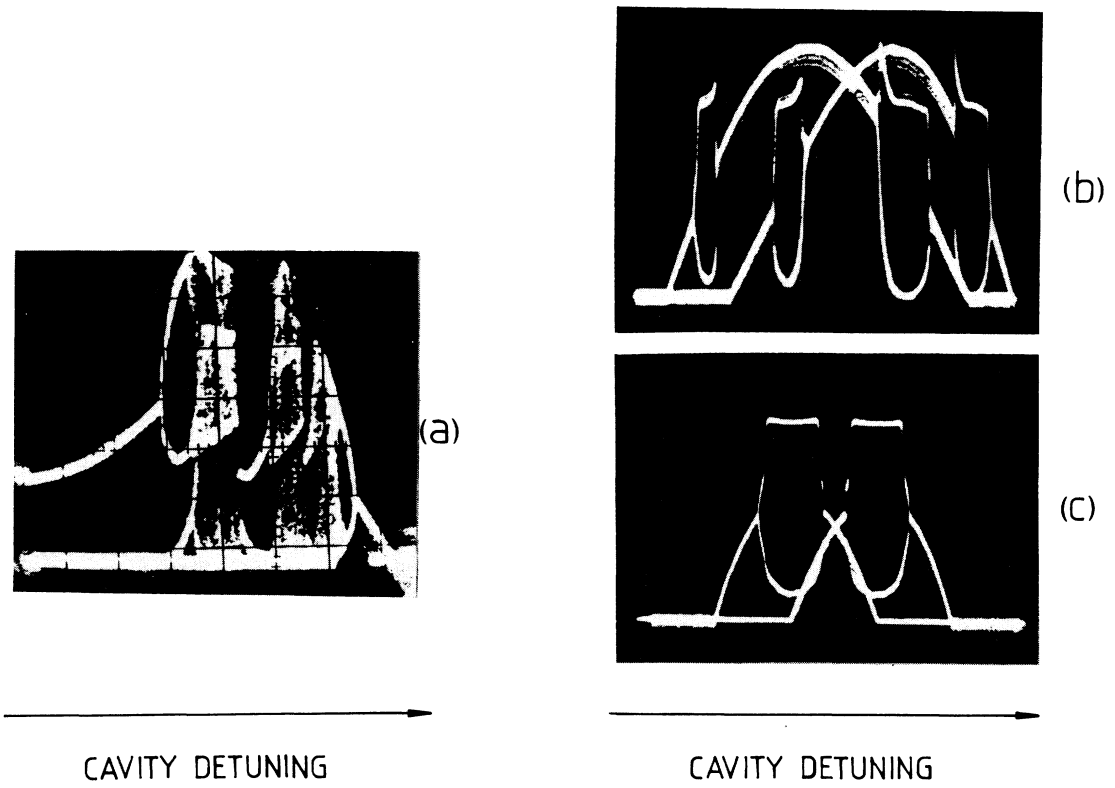

FIG. 8. Bifurcation diagrams obtained with the laser detuning as a control parameter for (a) high modulation amplitude and (b) and (c) low modulation amplitude. The most nonlinear regime has been obtained in the slope of the laser mode when the laser gain is low (c) and on top of the mode (zero detuning) when it is high (b). The detuning is swept over one mode width ($\sim$200 Mhz).

ally a T regime which is not shown on Fig. 8. The BD is symmetric with respect to central tuning but appears asymmetrical because of the nonlinearity of the PZT.

BD's obtained with smaller modulation amplitudes display more precisely the dependence of the regime on the detuning. In those presented on Fig. 8(b) and 8(c) only the $T \leftrightarrow 2T$ bifurcations occur when the laser frequency is swept. The mode pattern of the laser is clearly visible on these Figs. 8(b) and 8(c) where the two traces related to the backward and forward sweeps of the cavity length are shifted from one another because of the PZT hysteresis. The most nonlinear response occurs in the slope of the mode pattern ($2T$ regime) while the laser response is more linear (T regime) on the top and in the far wings [Fig. 8(b)]. In the conditions of Fig. 8(c), the cavity is slightly misaligned but the laser still oscillates monomode. Thus it may be assumed that only the loss rate of the cavity is changed. In this situation the sensitivity to nonlinearity is reversed and the largest nonlinearity is obtained for a laser cavity tuned to the center of the molecular line.

Numerical simulations will confirm that the loss rate of the cavity strongly affects the shape of the BD's—in particular, the most nonlinear points in the laser mode may move from the central frequency to the wings of the laser mode. The influence of the cavity detuning is also clear when BD's obtained by varying the modulation amplitude are compared for different values of this detuning. In these conditions three characteristic BD's are presented on Fig. 9. When the laser cavity is tuned at the center of the emission line [Fig. 9(a)], the diagrams exhibit a sequence T-$2T$-chaos without details in the subharmonic cascade or in the $3T$ regime. When the detuning is small ($\simeq$20 MHz) the $2T$ and $4T$ periods are easily seen and a large $3T$ regime appears [see Fig. 9(b)]. As the laser is detuned by about 100 MHz [Fig. 9(c)], the BD presents generalized bistability and sudden changes called "crises" as studied in more detail in Sec. VII and VIII.

All these examples show that the BD's are very efficient tools to characterize the various regimes of the CO_2 laser with modulated parameters. Because of the time scale of the phenomena in this laser system, they readily provide a large amount of results which should be compared with the predictions of the theoretical model.

VI. NUMERICAL SIMULATIONS

The results obtained with the experimental device are compared here with those derived from numerical simulation on the basis of the well-known two-level model previously discussed by many authors.[11,12,14,23] The behavior of the CO_2 laser can be described by a set of two coupled nonlinear differential equations:

$$\dot{I}=I\left[\frac{GD}{1+\delta^2}-2\kappa_0\right],$$
$$\dot{D}=\gamma_{\parallel}\left[1-D-\frac{DI}{1+\delta^2}\right]. \quad (1)$$

In these equations G is the gain and I and D are, respectively, the intensity and the population inversion. Their equilibrium values are $I_0=G/2\kappa_0-(1+\delta^2)$ and $D_0=(2\kappa_0/G)(1+\delta^2)$. κ_0 is the cavity damping rate and δ is the detuning from resonance expressed in units of the polarization relaxation rate $\gamma_{\perp}$.

Due to the reasons discussed in Sec. II, the elastooptic modulation mainly induces a loss modulation and κ is consequently written as a function of the frequency of the driving sine wave voltage as

$$\kappa=\kappa_0[1+m\sin(2\pi ft+\phi)], \quad (2)$$

where m is the modulation index. Then the nonautonomous differential system takes the following form:

$$\dot{I}=2\kappa_0 I\left[\frac{AD}{1+\delta^2}-1-m\sin(2\pi ft+\phi)\right],$$
$$\dot{D}=\gamma_{\parallel}\left[1-D-\frac{DI}{1+\delta^2}\right], \quad (3)$$

where $A=G/2\kappa_0$ is the pump parameter of the CO_2 laser.

The experimental parameters have been estimated to values which describe as well as possible our experimental situation. The frequency f is fixed at 400 kHz, the cavity damping rate κ_0 of our waveguide cavity is estimated to be 6.10^7 s^{-1}, and at 50 Torr the population relaxation rate $\gamma_{\parallel}$ is calculated to be 2.5×10^5 s^{-1} from the work by Dupré *et al.*[24] The usual value of the mode width of the laser is 200 MHz corresponding to $\delta=0.4$. In order to obtain a pump parameter just above 1 when $\delta=0.4$, the A parameter has to be fixed around 1.2. Practically, in numerical simulations, A has been varied between 1 and 1.2.

The equations have been numerically solved by the Merson's method with initial conditions given by the $m=0$ steady-state solutions. The calculated signal versus time is stored as soon as the transient is sufficiently damped, i.e., after a time corresponding to 100 periods of the driving signal.

Figure 10 shows the calculated signal when m is in-

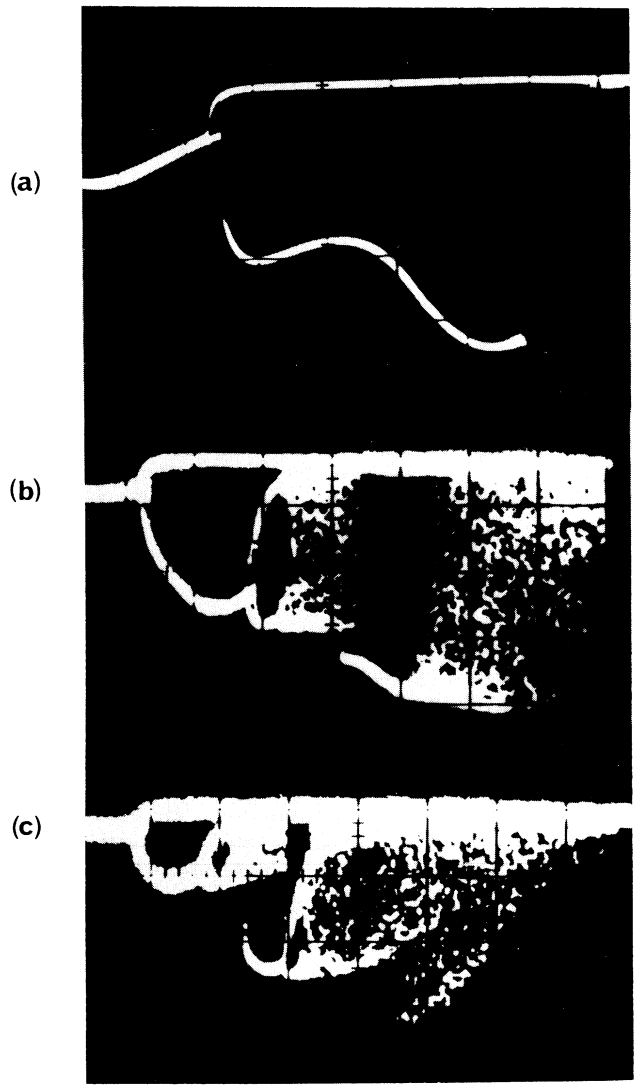

FIG. 9. Influence of the laser frequency on the BD obtained with the modulation amplitude as a control parameter in conditions of relatively low laser gain. The cavity detuning is, respectively, (a) 0, (b) 25, (c) 100 Mhz.

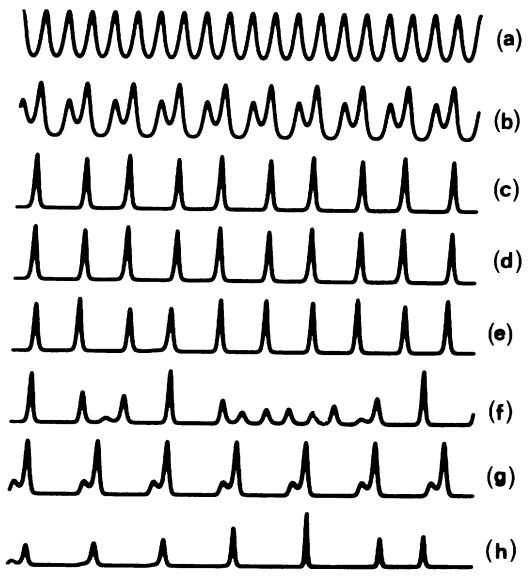

FIG. 10. Time dependence of the laser intensity calculated for the following values of the modulation index with $A=1.1$, $\epsilon=2.083.10^{-3}$, $f=400$ kHz, and $\delta=0$. (a) $m=0.01$, period 1; (b) $m=0.015$, period 2; (c) $m=0.02$, period 4; (d) $m=0.021\,27$, period 8; (e) $m=0.022$, chaotic signal (quasiperiodicity $2T$), (f) $m=0.0246$, chaotic signal; (g) $m=0.0337$, period 3; (h) $m=0.0338$, chaos.

creased from 0.01 (a) to 0.0338 (h). These different kinds of signals are in good agreement with the corresponding experimental recordings shown on Fig. 1, and the 2^nT cycles (a), (b), (c), and (d) are easily obtained as well as the $3T$ cycle (g). Chaos with quasiperiodicity 2^nT has also been found.

The best way to illustrate the simulated response of the laser is to build a BD by stroboscopic sampling of the laser intensity and of the population inversion at each period of the excitation signal when either m or δ are chosen as control parameters. Changing the phase ϕ allows the exploration of the intensity or of the population inversion variations during a period of the driving signal.

In order to reduce the integration time needed to obtain BD's, some transformations have been performed on the laser equations. The shape of the experimental signal suggests that at least at low m values, the intensity is approximately varying as the exponential of the sine wave modulation [see Fig. 10(a)].

Writing $I(t)$ as

$$I(t)=\frac{\gamma_{\parallel}(1+\delta^2)}{2\kappa_0}Y(t)\exp\left[\frac{m}{\pi f}\cos(2\pi ft+\phi)-\cos\phi\right], \tag{4}$$

the coupled equations take now the form

$$\dot{Y}=Y(D_1-1), \tag{5a}$$

$$\dot{D}_1=A_1-D_1[\epsilon+Y\cdot X(t)], \tag{5b}$$

where

$$\epsilon=\gamma_{\parallel}/2\kappa_0,$$

$$A_1=\epsilon A/(1+\delta^2),$$

$$D_1=DA/(1+\delta^2).$$

A_1 and D_1 are the reduced pump parameter and population inversion, respectively. In these equations the dot means time derivation with respect to the dimensionless time $t'=2\kappa_0 t$;

$$X(t)=\exp\left\{\frac{\kappa_0 m}{\pi f}\left[\cos\left[\frac{\pi ft}{\kappa_0}+\phi\right]-\cos\phi\right]\right\}$$

is the forcing term. If Equation (5b) is not modified, the first one takes now a simpler expression due to the fact that a part of the exponential contribution to the intensity is analytically included.

As an heuristic method, an iteration map may be used to predict some features that are likely to appear in the BD of the differential system. However, it should be kept in mind that there may be significant differences between the differential and the iterative systems.[20] Using a first-order Taylor expansion of Y and D_1 with respect to the dimensionless time t', the system takes now the form of a three-dimensional map:

$$Y_{n+1}=Y_nD_n,$$

$$D_{n+1}=A_1+D_n(1-\epsilon-Y_nX_n) \tag{6}$$

where the forcing term X_n is given by

$$X_n=\exp\left\{\frac{m\kappa_0}{\pi f}\left[\cos\left[\frac{\pi f}{\kappa_0}n+\phi\right]-\cos\phi\right]\right\}.$$

I_n is easily deduced from these equations.

This map does not correspond to a Poincaré section of the three-dimensional system since the dimension of the phase space is not reduced; it gives only a step-by-step ($1/N=f/2\kappa_0$) calculation of the solution as it is done, in fact, with numerical integration methods. For example, at low m values, the limit cycle of period 1 is covered in N iterations. Since N is 300 with the chosen experimental parameters, the first-order Taylor expansion of the modified differential system may be considered, at least at low m values, as a good approximation of the differential system. Note that it is not true if one uses the original system of Eq. (1).

Due to its simplicity, this three-dimensional map seems to be a useful tool and has been largely used on a personal computer for the analysis of the different types of response of the numerical system. However, it is certain that this iteration map does not give the same solutions for I and D as the differential system, but it has been verified that, for different sets of parameters, the two methods give quite similar BD's, except a systematic shift of the bifurcation points towards lower m values as shown on Fig. 11 which presents calculated BD's obtained by the two methods: (a) numerical solution of Eq. (3) and (b) map of the modified system as given by Eq. (6). Period-doubling bifurcations look very similar to the experimental ones. The only difference is the width of the $5T$ region. The discontinuity observed at the first bifurcation point is not due to a lack of convergence and will be explained in Sec. VIII. As δ is increased, it has been observed that the $5T$ region is first shifted towards lower m values, then gets narrower and disappears.

It has been shown experimentally in Sec. III that the laser frequency, which is related to the effective pump parameter A_1, has a strong influence on the BD pattern. An easy way to study this dependence is to calculate the BD with δ as a control parameter and to study its evolution for various m values. Figure 12 gives an example of BD when m is fixed to a value low enough ($m<0.01$) such that only one period doubling is achieved. These numerical simulations are in good agreement with the experimental work (see, e.g., Fig. 8). It appears in the calculations that the limit cycle representing the laser response loses its stability to give a cycle of period 2 when one reaches a value of δ such that the dimensionless eigenfrequency of the system

$$\lambda=\frac{1}{2\pi}\left[2\kappa_0\gamma\left[\frac{1}{1+\delta^2}-1\right]\right]^{1/2}$$

is near one-half. When κ_0 is increased, δ is consequently decreased in good agreement with the experimental study in which it is possible to vary κ_0, for instance, by the choice of the operating cavity mode of the laser.

Figure 12(a), calculated with $A=1.11$, shows that the response of the system is again T periodic when δ is near zero. On the other hand, when A is decreased to 1.06

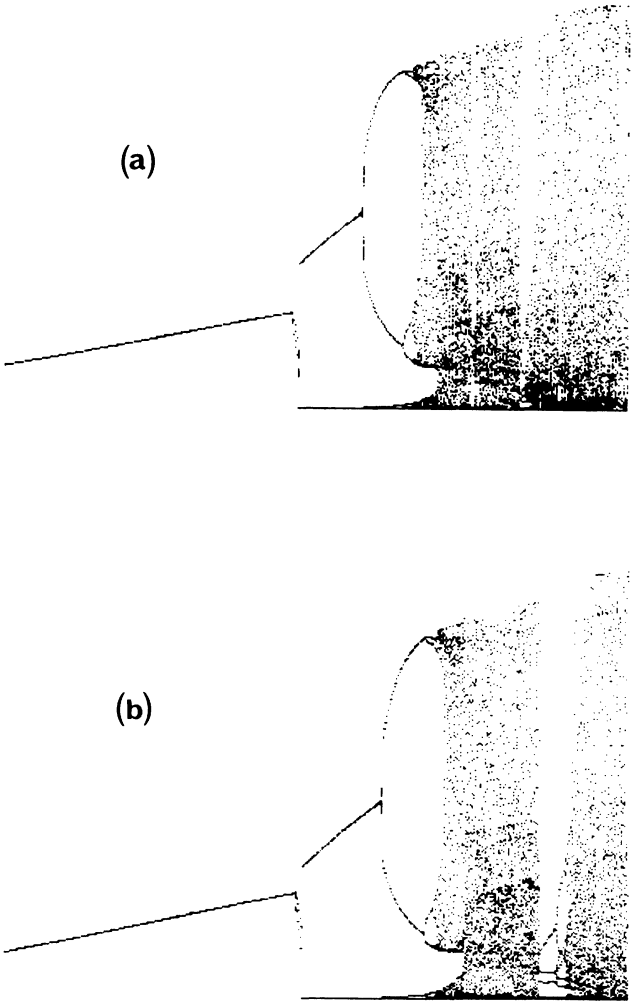

FIG. 11. Calculated BD's in the AM mode for $A=1.1$, $\epsilon=2.083.10^{-3}$, $f=400$ kHz, and $\delta=0.08$ vs m as a control parameter using (a) the iteration map, (b) the differential system. m is increased from 0 to 0.03.

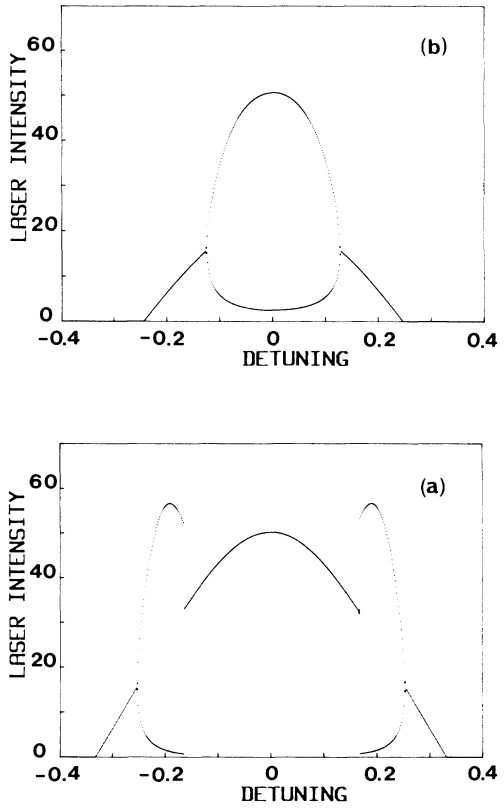

FIG. 12. Calculated BD in the AM mode vs δ as a control parameter for (a) $A=1.11$, $m=0.011$; (b) $A=1.06$, $m=0.011$. Other parameters as in Fig. 11.

[Fig. 12(b)], its response remains $2T$ periodic even for $\delta=0$. This behavior will be discussed in Sec. VII.

As has been shown in Sec. II, the elasto-optic modulator induces not only a loss modulation (AM) but also a frequency modulation (FM) of the laser. It appears that the latter is much less efficient at least at low modulation amplitudes; this confirms an earlier theoretical prediction.[3] Nevertheless, in the FM mode, the modulation should be the most efficient the larger the cavity detuning is. Numerical simulations using the same simplified model as in Eq. (1) have been performed to set the qualitative differences between the BD's, with δ written as

$$\delta=\delta_0+m\delta_1\sin 2\pi ft \ ,$$

where δ_1 is the half width of the laser cavity mode. They show no qualitative difference with the corresponding diagrams obtained with loss modulation except a much lower efficiency of the FM mode, about one order of magnitude with our set of parameters.

VII. GENERALIZED MULTISTABILITY

We have observed experimentally that when the detuning δ is of the order of one half the mode width, the BD is much more complicated than the one obtained from the logistic map. In fact, the behavior of the laser sometimes depends not only on the parameters but also on their previous history. This is the phenomenon of generalized multistability which was previously predicted by Matorin *et al.*[14] and by Solari *et al.*[25] and observed by Arecchi *et al.*[2,26,27] and Dangoisse *et al.*[22] in lasers with periodic modulation. Figure 13 shows two BD's recorded when the amplitude modulation is linearly (a) increased or (b) decreased. The scenario is qualitatively the same in the two recordings. The period-doubling cascade clearly appears as well as a $3T$-periodic "window" inside the chaotic region. These BD's look clearly different in the region of chaos and $3T$-periodic "windows" depending on whether the control parameter is increased or decreased. More specifically, in bifurcation diagrams obtained by increasing the modulation amplitude, a narrow $3T$ window follows a relatively

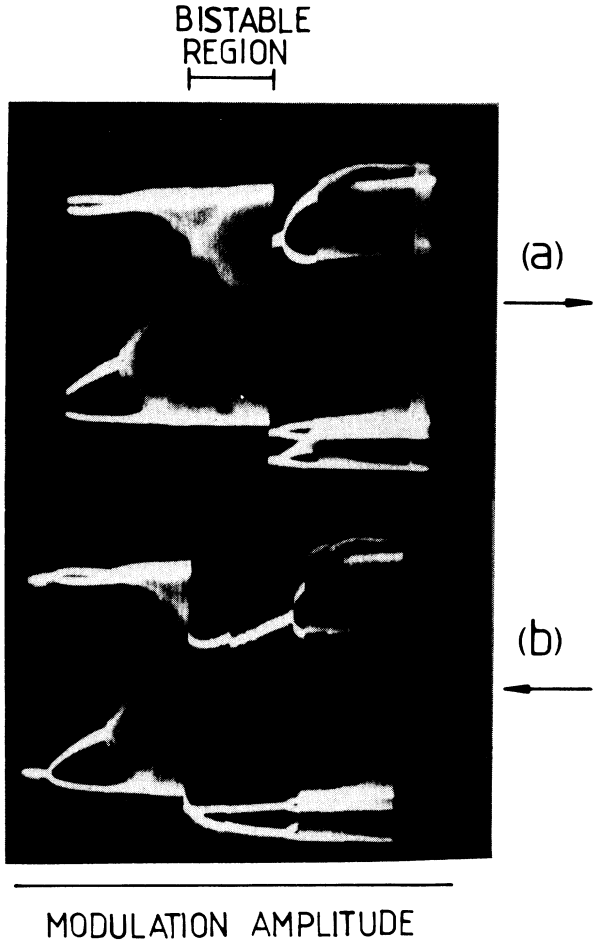

FIG. 13. Experimental evidence of GB between the $3T$ and the chaotic regime obtained in increasing (top) or decreasing (bottom) the driving amplitude. The $3T$ "window" is much wider in (b).

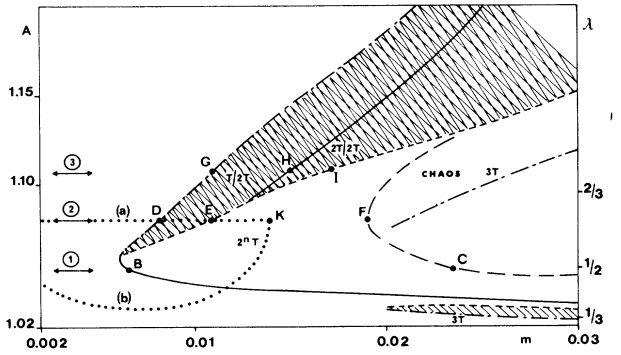

FIG. 14. Attractors map showing some of the different coexisting regimes obtained with the iteration map in the (A,m) phase plane. The other parameters are the same as in Fig. 11. This diagram may be explored in different ways as follows:

(1) By increasing m from 0, period 2 is reached at point B and chaos in C after period-doubling bifurcations. The —— line refers to a T-$2T$ bifurcation.

(2) Again by increasing m, period 2 is reached in E in a "discontinuous" bifurcation and chaos in F after period-doubling bifurcations. Coming backward from F, the system remains in period 2 until D is reached, where it recovers the initial period-1 limit cycle. At each point of the —·—·—· lines a saddle-node bifurcation may occur. The — — — line corresponds to a discontinuous bifurcation.

(3) Period 2 is reached in H in a normal bifurcation. In I the system jumps on a new period-2 limit cycle after a discontinuous bifurcation. From I, in the backward direction, the limit cycle of period 2 is observed until G is reached. The bistability region is marked with double hatchings.

Note that the same regime may be obtained through continuous or discontinuous transitions as illustrated by the dotted lines. Path (a) Period 2 is reached at point K after a discontinuous bifurcation, path (b) The same period-2 limit cycle is achieved following a "normal" bifurcation.

broad chaotic region with quasiperiodicity $2T$, while when the sweep is reversed, the $3T$ window is extended to a range of the modulation amplitude m where the system was chaotic during the forward sweep. Thus for some range of m, there is a "generalized bistability" (GB) between the "noisy" $2T$ and $3T$ regimes. The width of this bistability region depends on the laser frequency as shown on Fig. 3. However, the bistability is not measurable when the laser cavity is tuned on the top of the gain profile and the GB appears rather when the cavity is detuned by about 100 MHz. The bistable region broadens while increasing the detuning and can even cover up the whole chaotic region resulting in an almost direct transition from the $3T$ window to the $8T$-$4T$-$2T$ sequence. By selection of the laser mode, it has also been experimentally observed that GB disappears when the laser operates with high losses.

GB, which is observed only when two attractors are coexisting, indicates that at least two attractors are present for some values of the experimental parameters. A numerical study has been undertaken to characterize these various attractors as a function of the control parameters. In this study we have obtained the different solutions for I and D when the pump parameter and the modulation index are varied, i.e., in the (A,m) phase plane, using the three-dimensional map described in Sec. VI. Checks have been regularly made to ensure that the map and the differential equations (1) provide very similar BD's. The range of variation of A and m are limited to values below 1.2 and 0.03, respectively. All the limit cycles are calculated in the same conditions: For given values of m and A (or λ), the map is iterated so as to obtain its limits with a given accuracy, the initial conditions being provided by the limit found for the previous m (or A) value when A (or m) is fixed. The results of this study are schematically represented in Fig. 14. It is shown that the limit cycle of period T (period 1 attractor) is, if not destroyed, elsewhere in the plane, a solution of the system. In fact, with increasing the modulation index m while A is kept constant, this limit cycle loses its stability and gives rise to chaos via a sequence of period-doubling bifurcations. The λ parameter ap-

pears to be a determinant factor in the behavior of the system. When A is fixed and m varied step by step, the passage to period 2 is obtained for the smallest m value when λ is near one half ($A=1,053$). Figure 14 shows also the dashed lines corresponding to the first period-doubling bifurcation for the period-1 attractor. Two cases have to be considered: when λ is less than one half, period 2 is achieved via a "normal" bifurcation similar to that of the logistic map. On the contrary, when λ is greater than one half, the system is attracted by a period-2 attractor which is a limit cycle of period 2 born in a saddle-node bifurcation. This saddle-node bifurcation creates simultaneously an attracting period-2 orbit as well as an unstable period-2 orbit. The coexistence of attractors in the same laser system has recently been discussed in details by Solari *et al.*[25] We have observed GB between the period-1 and -2 attractors as is shown on Fig. 15. This behavior explains the appearance of a discontinuity in the BD of Fig. 11 when m is increased. In fact, it is not due to a "normal" bifurcation but to a jump from a limit cycle of period T to another one with period $2T$ born previously in a saddle-node bifurcation. For m values in the range 0.008–0.012, the two attractors coexist for the same values of the parameters. If m decreases, the system stays on the period-2 attractor before "falling down" on the period-1 attractor near the point where the saddles and nodes annihilate (see Fig. 15). Beyond these points, the period-2 attractor no longer exists. When m is kept constant, the BD calculated while increasing (or decreasing) A looks like a closed loop similar to the remerging Feigenbaum trees[26–28] but exhibiting a discontinuity with associated GB as the system falls (or jumps) from period 2 (1) to period 1 (2). When A and m are simultaneously varied, it has been checked that the system may go from the point ($A,m=0$) to ($A,m=0.014$) without encountering any discontinuity in the BD [route (b) in Fig. 14] contrarily to the previous description

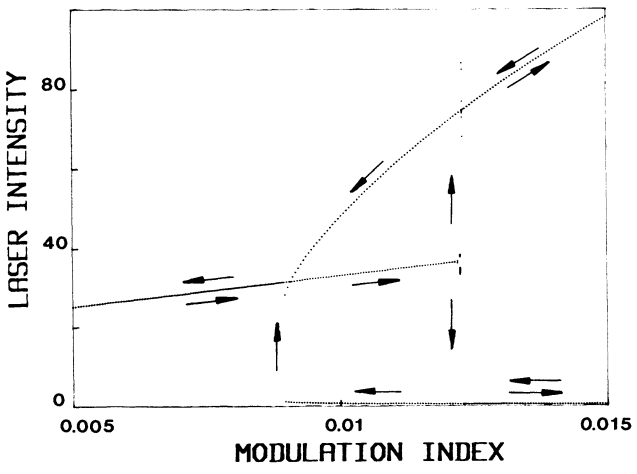

FIG. 15. Numerical evidence of GB between the T and $2T$ regime obtained with the iteration map. m is increased and decreased between 0.005 and 0.015 with $A=1.1$, $\delta=0.12$. The other parameters are left unchanged.

[route (a)]. In the regions where $\lambda=n/3$ with $n=1,2$, saddle-node bifurcations giving rise to period-3 attractors have also been detected. These attractors lose their stability via period-doubling sequences as m is increased. The only way to jump to period-3 attractor is to choose the initial conditions in its basin of attraction. When $\lambda=\frac{2}{3}$ the period-3 attractor coexists with the chaotic region of the period-2 attractor. Period-5 attractors may also appear in the BD as a function of m. For instance, one of them is visible in the region near $A=1.1$ and $m=0.015$ in Fig. 11. We have not tried to detect attractors other than those described here, but "hidden" coexisting attractors could appear with an adequate choice of the initial conditions. It seems and it should be checked carefully that the behavior of the system is qualitatively the same when using other sets of parameters for ϵ and f.

A few checks have been performed for comparison with the differential system. They show that in the range of parameters investigated in this study, its behavior is qualitatively the same.

If $\gamma_{\parallel}$ is varied when f and κ_0 are kept constant, the λ scale is then shifted with respect to the A scale, thus all the positions where the different attractors interact should be modified and period-3 attractors should appear in the BD after a collision with unstable limit cycles. The map of Fig. 14 is of great help for the interpretation of the BD's obtained as a function of the control parameters m and δ. For instance, the interpretation of the BD versus δ (see Fig. 12) is the following: When increasing δ ($\delta<0$) or λ, the system is first on a limit cycle of period 1 which gives rise via a period-doubling bifurcation, as explained above, to a limit cycle of period 2 before going back on the period-1 limit cycle resulting in a closed loop also called "remerging" Feigenbaum trees.[28–31] The same scenario is reproduced for the positive values of δ. According to the m value, the BD has either simple loops ($m<0.012$), or more complicated ones ($m>0.019$) in which the system undergoes successive period-doubling bifurcations and possibly becomes chaotic, before going back to the period-T limit cycle in the opposite way when δ is decreased to zero.

In the case where the pump parameter is reduced to 1.06, the system goes from a period-1 attractor to a period-2 attractor and remains on a period-2 attractor when the system is tuned at exact resonance ($\delta=0$). As a result, for small m values, the BD exhibits only one closed loop on the top of the mode contour of the laser.

VIII. CRISES

As was pointed out by Greboggi, Ott, and Yorke, the evolution of attractors born in saddle-node bifurcations gives rise to crises.[32,33] A crisis is a sudden change in the behavior of an attractor. Crises are characterized by a collision between a chaotic attractor and an unstable fixed point or periodic orbit. When this orbit is just at the boundary of the basin of attraction of the chaotic attractor, the crisis is called a boundary crisis. On the contrary, if the unstable periodic orbit is inside the basin

of attraction, the crisis is called an interior crisis. The attractor and its basin of attraction are simultaneously destroyed by a boundary crisis. On the opposite, in an interior crisis one observes only a sudden expansion of the explored region of the phase space, since regions previously located outside the attractor are now visited. Such crises were observed in model electronic circuits by Hilborn[34] and by Rollins and Hunt[35] and should be distinguished from noise-induced jumps between different coexisting attractors.[36–38]

We report in this section on the observation and characterization of different crises on attractors in an AM CO_2 laser, previously described in Ref. 7. Then numerical simulations in good qualitative agreement with the experimental recordings will be presented. As mentioned above, the effect of boundary and interior crises on a chaotic attractor are different and this allows us experimentally to distinguish clearly between the two kinds of crisis. The BD, as well as the phase diagrams in which the laser output I is displayed versus its time derivative $\dot{I}$, proved useful in the investigation of crises. In the last representation, a crisis is revealed by a sudden appearance of new explored regions in the $(I,\dot{I})$ plane.

Let us first discuss the crisis giving rise to the $3T$-periodic regime (see Fig. 11). This $3T$-periodic regime is not the normal periodic window surging by a tangent bifurcation inside the chaotic domain.[18]

This statement is supported by three experimental facts: (i) there are conditions in which generalized bistability between the chaotic attractor and the $3T$ limit cycle exists, (ii) the width of the region in which the $3T$ regime occurs is much broader than that associated with the usual $3T$-periodic window (for instance in the logistic map), and (iii) the sampled values in the $3T$ regime are often well outside the region visited by the chaotic attractor. This statement is confirmed by the numerical simulations reported above which show that this "periodic window" is, in fact, a period-3 attractor. The appearance of the $3T$ attractor follows a boundary crisis which destroys not only the $2T$ attractor but also its basin of attraction.

Different situations of crises have been observed as the cavity detuning is varied. They appear as expansions of the attractor but not as its destruction and consequently are interior crises. When the laser is only slightly detuned from resonance, at some critical value of the control parameter a new branch appears in between the two branches previously visited by the system (see Fig. 16). Another illustration of this crisis is given by the $[I(t),\dot{I}(t)]$ diagram in the vicinity of this event as displayed on Fig. 17. The evolution of the laser attractor in the experimental conditions of these diagrams is summarized in the lower part of this figure. After the period-doubling cascade, the attractor becomes chaotic for a modulation amplitude $V_{\text{mod}}=185$ mV. As V_{mod} is increased, the attractor evolves smoothly until it reaches the critical value $V_{\text{crisis}}=204$ mV where a new branch of the phase diagram suddenly appears in between the two main branches. As V_{mod} increased further, the laser attractor follows more and more frequently this branch which appears brighter in Fig. 17. Eventually this new

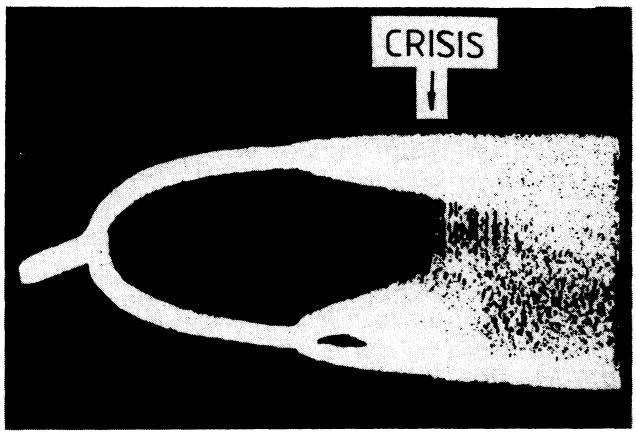

FIG. 16. Experimental display of a BD showing a period-doubling sequence to chaos and a crisis leading to an expansion between the two branches of the chaotic regime.

branch and the two main branches before the crisis smear out together. When the modulation is increased further, the laser jumps to the $3T$-periodic regime in the boundary crisis discussed above and later on again to chaos. When the modulation amplitude is decreased, the $3T$-periodic cycle region broadens and extends to a modulation range where the laser was previously chaotic. This is the GB effect discussed above, and a crisis is also observed when V_{crisis} is reached from above. In Fig. 17(c) it is shown that the region in between the upper and lower chaotic branches is not evenly explored just after the crisis. This does not appear in Fig. 16 because that photograph was mainly overexposed to show more clearly the new (intermediate) branch.

When the detuning of the laser frequency is large, a third situation of crisis is observed. The corresponding scenario is illustrated by Fig. 2 of Ref. 7. After the

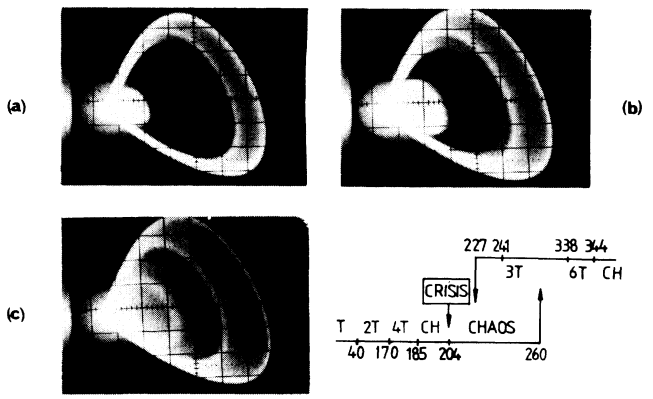

FIG. 17. $(I,\dot{I})$ plot in the crisis region at (a) 200 mV, (b) 204 mV, and (c) 208 mV driving voltages. The crisis is the same as that displayed in Fig. 16. (d) The situation of the crisis with respect to the "bistable" region is shown in the lower right part.

period-doubling sequence the regime becomes chaotic and for a critical value of the control parameter, the explored region of the phase diagram expands suddenly.

Figure 18 shows the evolution of the rebuilt $[I(t),I(t+\tau)]$ attractor. As the initial attractor is not destroyed, one could conclude that we are concerned with an interior crisis. A more detailed analysis of this crisis can be undertaken easily. The assignment of the observed changes of the BD to an internal crisis due to a collision of the chaotic attractor with unstable periodic cycles is supported by the direct observation of the time dependence of the laser intensity just after the crisis. This is particularly clear in the case of the crisis reported in Fig. 19 where the newly explored branches of the attractor correspond to intensity peaks much larger than the original $2T$ chaotic regime.

Then, as shown in Fig. 4 of Ref. 7, this original chaotic regime is interrupted by intermittent bursts of (quasi)periodic pulsations. At some irregular times, the laser temporarily jumps into a $5T$ unstable cycle regime, until it is eventually trapped again in the chaotic $2T$ attractor. Due to the narrowness of the crisis region this behavior has been distinguished from a noise-induced crisis.[36–38] In the conditions of this figure, the two regimes (chaotic $2T$ and $5T$ unstable cycle) are easily distinguished because they correspond to spikes with quite different intensities. This behavior is also illustrated in Fig. 5 of Ref. 7, which is a kind of return map showing the transition between the two regimes. It is associated to the crossing of the attractor with the plane $I=0$ since the amplitude of the nth maximum I_n is plotted versus that of the next maximum I_{n+1}. For driving amplitude V less than the crisis value, all (I_n,I_{n+1}) points remain located on a "curve" as shown in Fig. 5(a) of Ref. 7. When V is increased, this "curve" expands. As $V=V_c$, it reaches a point where the system escapes the $2T$ chaotic attractor. It explores points well outside the region shown in the figure. A typical scenario near the critical point is illustrated in Fig. 5(b) of Ref. 7 where the numbers indicate the chronology of the crisis and refer to the successive values of n. From points 3, 4, and 5, the system evolves on various limits of the "$2T$ attractor." From point 9, it is well outside the attractor.

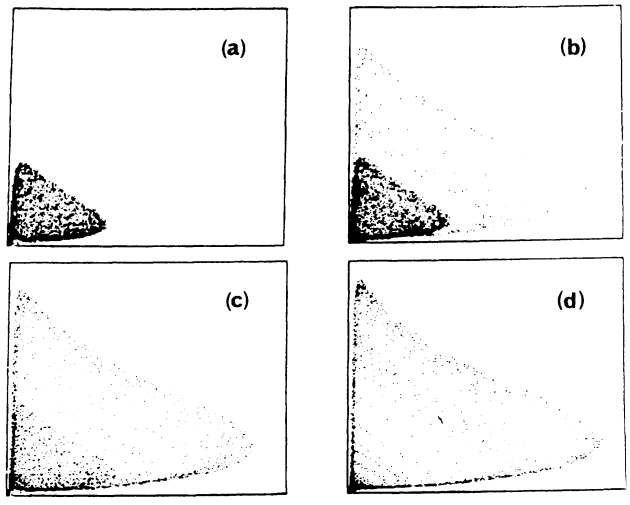

FIG. 18. Evolution of the $[I(t),I(t+\tau)]$ phase diagram, shown, respectively, (a) before, (b) and (c) during, (d) after the crisis.

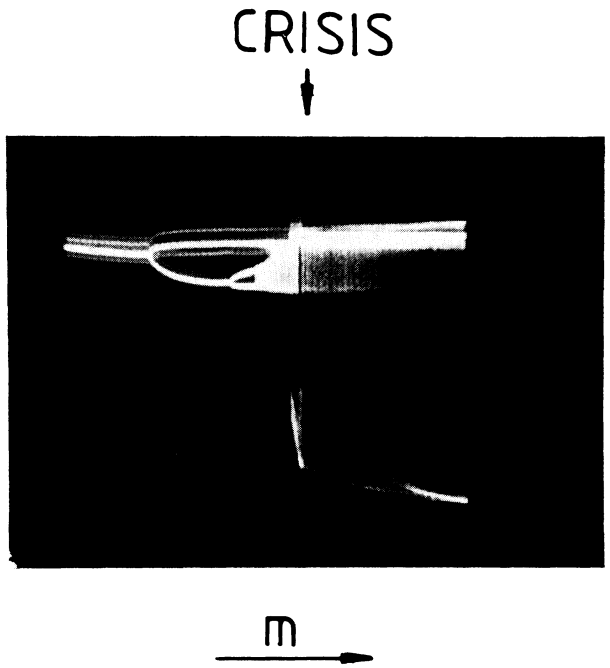

FIG. 19. Experimental BD in a large range of variation of the driving voltage. The crisis corresponds here to a sudden expansion of the chaotic attractor.

The experimental investigation of a number of crises of this kind indicates that the scenario is always the same for different bursts of nT-pseudoperiodic pulses and thus may be considered as a signature of the particular crisis under investigation.

IX. DYNAMICAL EFFECTS

Up to now we have considered that the experimental observations were made at constant control parameter. In fact, if one wants to observe BD's, a slow sweep of the control parameter is needed. The aim of this section is to study the alteration of the BD's produced by the slow variation of the control parameters. Due to the hysteresis of the PZT used to sweep the cavity length, only the modulation index has been used as a control parameter in the following experimental results.

We have more particularly studied the influence of the sweep rate on the first bifurcation $T\rightarrow 2T$. Figure 20 shows three different recordings obtained for the sweep frequencies of 3 Hz, 30 Hz, and 300 Hz, respectively. A voltage plateau at the end of each sawtooth allows the system to recover the stationary state before applying the next sweep in the backward direction. Even at the lowest frequency, one notices differences between the

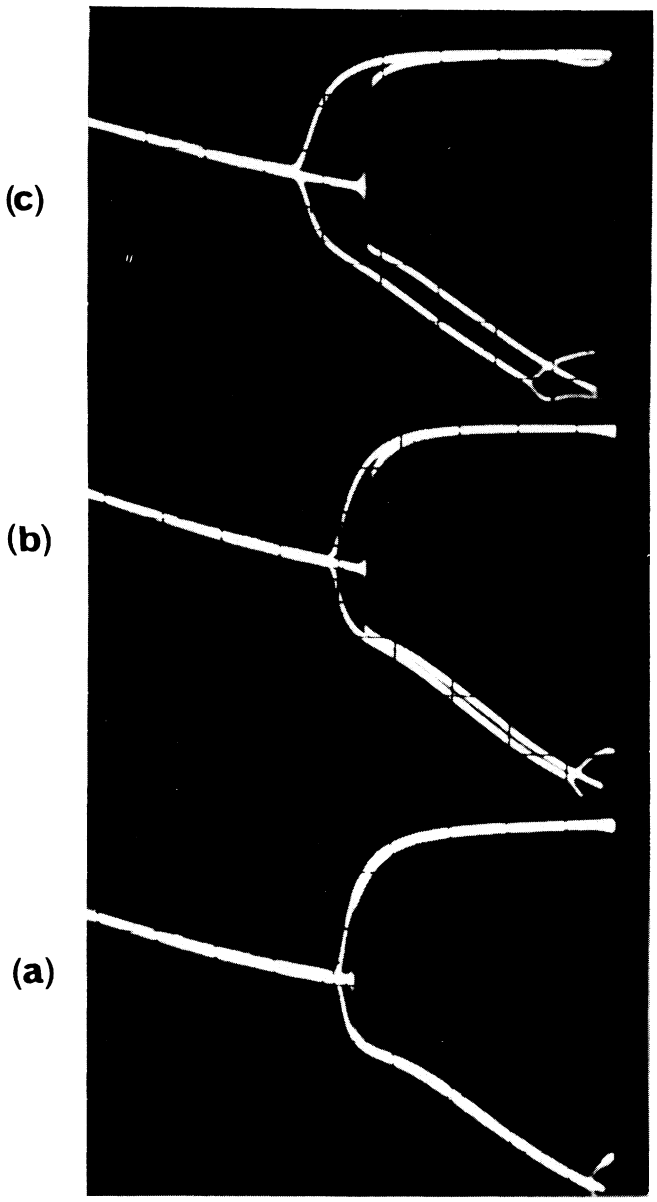

FIG. 20. Influence on the T-$2T$ bifurcation of the sweep frequency (a) 3 Hz, (b) 30 Hz, and (c) 300 Hz.

direct and reverse traces.

The experimental study shows that at least three different types of dynamical effects are induced by the sweep of the control parameter.

(1) A dynamically induced bistability which appears as follows: with increasing the modulation amplitude, the T-periodic solution is first dynamically stabilized, then the system jumps suddenly on the $2T$ trajectories, while the reverse happens with the decrease of the amplitude modulation; the $2T$-periodic regime is during a short time dynamically stabilized, then the system moves back slowly towards the T-periodic regime. Preliminary results show that the width of the dynamically induced bistable zone evolves as the square root of the sweep rate of the control parameter as predicted by Kapral and Mandel on the nonautonomous logistic map.[39]

(2) A very asymmetric shift of the branches of the BD. This effect is particularly evident on the lower branch of the BD shown on Fig. 20. This shift varies also with the sweep rate of the control parameter, in a similar way to the corresponding effect observed with the logistic map.

(3) Dynamical effects also arise in presence of GB in a similar way to those appearing in bistability between fixed points.[40–42] The commutation points are dynamically shifted and the width of the bistable region broadens notably together with the increase of the sweep rate. For instance, the $3T$-periodic regime, which is hardly observed with the increase of the amplitude modulation, becomes considerably broader and fills a larger part of the BD when the amplitude modulation is decreased.

All these different effects have generally the same dependence with the sweep rate of the control parameter as that observed with the nonautonomous logistic map or with the differential system described in Sec. VI. The

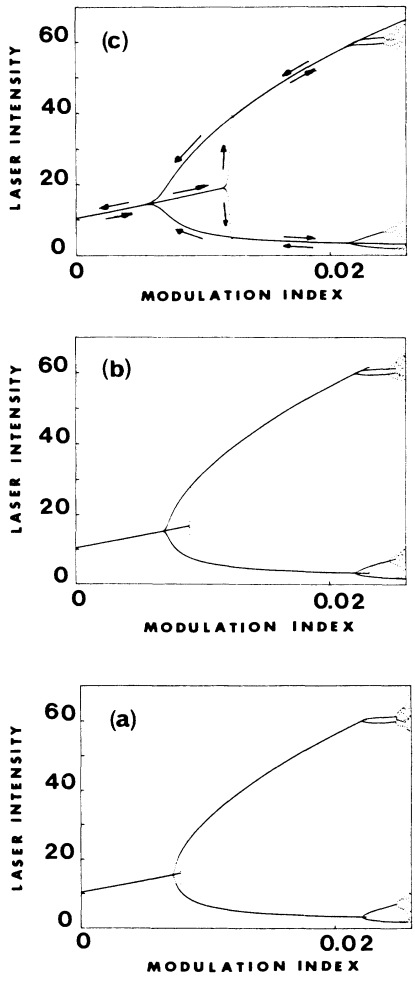

FIG. 21. Calculated BD's for $A=1.05$ and $\delta=0$ when m is swept as in Fig. 20. Other parameters as in Fig. 11.

differential system has been solved, keeping unchanged all the parameters except A fixed at a value (1.05) for which static GB does not appear. Figure 21 shows the forward and backward BD's calculated in the conditions of Fig. 20, i.e., with almost the same values of the sweep frequency of the amplitude of the modulation index, fixed at 3.3 Hz, 30 Hz, and 333 Hz, respectively. All these diagrams show some common properties in good agreement with the experimental recordings. The forward BD exhibits an abrupt jump from period 2^nT to period $2^{n+1}T$ with possibly an overshot at very high speeds, while the backward transition from period $2^{n+1}T$ to 2^nT is rather smoothed. But, except in the region of induced bistability, the forward and backward BD obtained at a given sweep frequency are quite superimposed contrarily to the experimental ones. Even at low speed rate [Figs. 20(b) and 20(c)], the speed effects are only noticeable in the vicinity of the bifurcation points since the other points of the BD's keep almost the same amplitude independently of the sweep rate.

X. CONCLUSION

The direct observation of the bifurcation diagrams of the CO_2 laser with periodically modulated parameters provides an easy and efficient way to investigate the different regimes of this system and more particularly those in which the laser output is chaotic. In particular, generalized bistability, crises, and swept-parameter-induced postponement of bifurcations have been studied in this laser. Most of the phenomena which have been observed are in good agreement with numerical simulations based on a rate equation model of the laser.

The CO_2 laser with modulated losses appears as a convenient system for studying chaotic effects because of its high signal-to-noise ratio and because of the time scale of the phenomena to carry experiments which would be extremely difficult in other experimental domains. It is also a rich system displaying a wide variety of behaviors and new results are still expected, especially in the domain of generalized bistability and noise-induced transitions.

ACKNOWLEDGMENTS

The financial support of Direction des Recherches et Etudes Techniques (DRET) and La Région Nord, Pas de Calais, are gratefully acknowledged. Experiments were made possible by the loan of material from the Société Anonyme de Télécommunications—in particular, Michel Ouhayoun, Thierry Midavaine, and Philippe Jacquier who designed the laser and the elasto-optic modulator. The authors also benefited from fruitful discussions with J. R. Tredicce. The Laboratoire de Spectroscopie Hertzienne is associé au Centre National de la Recherche Scientifique.

[1]E. Arimondo and P. Glorieux, Appl. Phys. Lett. **33**, 49 (1978).
[2]F. T. Arecchi, R. Meucci, G. P. Puccioni, and J. R. Tredicce, Phys. Rev. Lett. **49**, 1217 (1982).
[3]J. R. Tredicce, N. B. Abraham, G. P. Puccioni, and F. T. Arecchi, Opt. Commun. **55**, 131 (1985).
[4]G. P. Puccioni, A. Poggi, W. Gadomski, J. R. Tredicce, and F. T. Arecchi, Phys. Rev. Lett. **55**, 339 (1985).
[5]T. Midavaine, D. Dangoisse, and P. Glorieux, Phys. Rev. Lett. **55**, 1989 (1985).
[6]J. R. Tredicce, F. T. Arecchi, G. P. Puccioni, A. Poggi, and N. Gadomski, Phys. Rev. A **34**, 2073 (1986).
[7]D. Dangoisse, P. Glorieux, and D. Hennequin, Phys. Rev. Lett. **57**, 2657 (1986).
[8]Y. C. Chen, H. G. Winful, and J. M. Liu, Appl. Phys. Lett. **47**, 208 (1985).
[9]W. Klische, H. R. Telle, and C. O. Weiss, Opt. Lett. **9**, 561 (1984).
[10]E. Brun, B. Derighetti, D. Meier, R. Holzner, and M. Ravani, J. Opt. Soc. Am. B **2**, 156 (1985).
[11]P. A. Khandokhin and Ya. I. Khanin, Kvant. Electron. (Moscow) **11**, 1483 (1984) [Sov. J. Quantum Electron. **14**, 1004 (1984)].
[12]D. V. Ivanov, Ya. I. Khanin, I. I. Matorin, and A. S. Pikovsky, Phys. Lett. **89A**, 229 (1982).
[13]T. Erneux, S. M. Baer, and P. Mandel, Phys. Rev. A (to be published).
[14]I. I. Matorin, A. S. Pikovskii, and Ya. I. Khanin, Kvant. Electron. **11**, 2096 (1984) [Sov. J. Quantum Electron. **14**, 1401 (1984)].
[15]A. Yariv, *Quantum Electronics* (Wiley, New York, 1975).
[16]J. P. Eckmann, in *Comportement chaotique des systèmes déterministes,* Les Houches, Session XXXVI, 1981, edited by G. Iooss, R. H. G. Helleman, and R. Stora, Electron. **QE-21**, (North-Holland, Amsterdam, 1983).
[17]J.-P. Eckmann and D. Ruelle, Rev. Mod. Phys. **57**, 617 (1985).
[18]P. Bergé, Y. Pomeau, and C. Vidal, *L'ordre dans le chaos* (Herman, Paris, 1984).
[19]M. W. Derstine, H. M. Gibbs, F. A. Hopf, and L. D. Sanders, IEEE J. Quantum Electron. **QE-21**, 1419 (1985).
[20]N. H. Packard, J. P. Crutchfield, J. D. Farmer, and R. S. Shaw, Phys. Rev. Lett. **45**, 712 (1980).
[21]J. D. Farmer, Z. Naturforsch, Teil A **37**, 1304 (1982).
[22]D. Dangoisse, P. Glorieux, and D. Hennequin, Proc. Soc. Photo.-Opt. Instrumen. Eng. **667**, 242 (1986).
[23]D. Dangoisse and P. Glorieux (unpublished).
[24]T. Dupré, F. Meyer, and C. Meyer, Rev. Phys. Appl. **10**, 285 (1975).
[25]H. G. Solari, E. Eschenazi, R. Gilmore, and J. R. Tredicce (unpublished).
[26]F. T. Arecchi, *Optical Chaos,* edited by J. Chrostowski and N. B. Abraham, Proc. SPIE **667**, 139 (1986).
[27]F. T. Arecchi, in *Optical Instabilities,* edited by R. W. Boyd, M. G. Raymer, and L. M. Narducci (Cambridge University Press, Cambridge, England, 1986), p. 183.
[28]M. Bier and T. Bountis, Phys. Lett. **104A**, 239 (1984).
[29]E. Knobloch and N. O. Weiss, Physica **9D**, 379 (1983).
[30]G. L. Oppo and A. Politi, Phys. Rev. A **30**, 435 (1984).

[31]D. Dangoisse and P. Glorieux, Phys. Lett. **116A**, 311 (1986).
[32]C. Grebogi, E. Ott, and J. A. Yorke, Phys. Rev. Lett. **48**, 1507 (1982).
[33]C. Grebogi, E. Ott, and J. A. Yorke, Physica (Amsterdam) **7D**, 181 (1983).
[34]R. C. Hilborn, Phys. Rev. A **31**, 378 (1985).
[35]R. W. Rollins and E. R. Hunt, Phys. Rev. A **29**, 3327 (1984).
[36]A. S. Pikovsky, Z. Phys. B **55**, 149 (1984).
[37]F. T. Arecchi and A. Califano, Phys. Lett. **101A**, 443 (1984).
[38]F. T. Arecchi, R. Badii, and A. Politi, Phys. Lett. **103A**, 3 (1984).
[39]R. Kapral and P. Mandel, Phys. Rev. A **32**, 1076 (1985).
[40]P. Glorieux and D. Dangoisse, IEEE J. Quantum Electron. **QE - 31**, 1486 (1985).
[41]E. Arimondo, G. Gabbanini, E. Menchi, D. Dangoisse, and P. Glorieux, in *Optical Instabilities,* edited by R. W. Boyd, M. G. Raymer, and L. M. Narducci (Cambridge University Press, Cambridge, England, 1986).
[42]E. Arimondo, C. Gabbanini, E. Menchi, and B. Zambon, *Optical Chaos,* edited by J. Chrostowski and N. B. Abraham, Proc. SPIE **667**, 234 (1986).

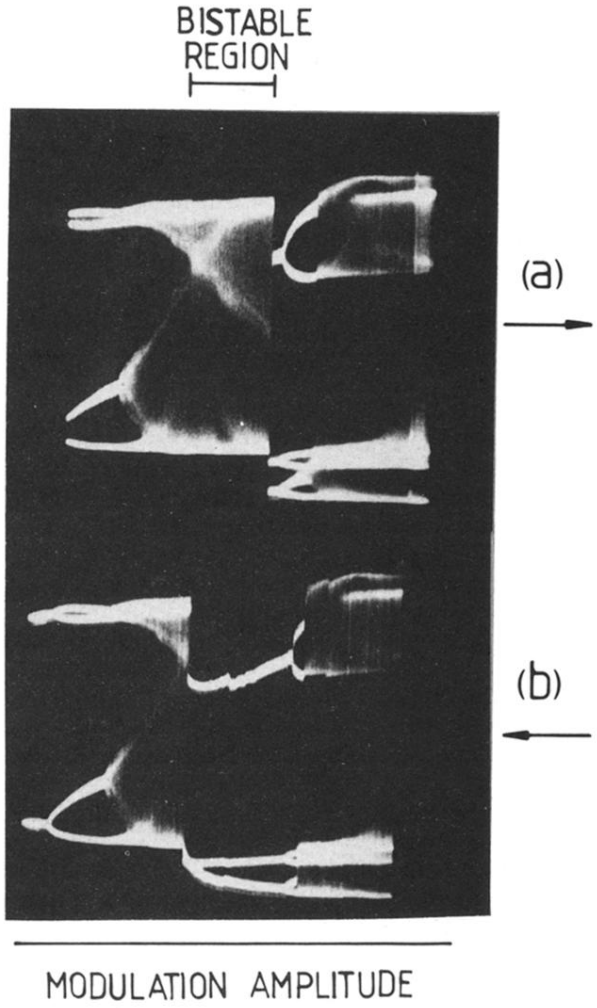

FIG. 13. Experimental evidence of GB between the $3T$ and the chaotic regime obtained in increasing (top) or decreasing (bottom) the driving amplitude. The $3T$ "window" is much wider in (b).

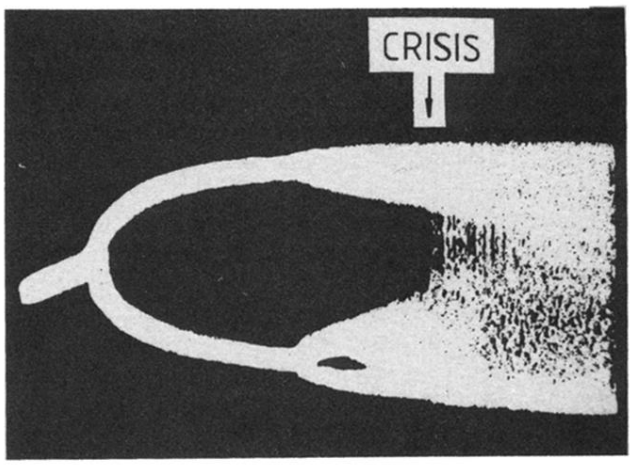

FIG. 16. Experimental display of a BD showing a period-doubling sequence to chaos and a crisis leading to an expansion between the two branches of the chaotic regime.

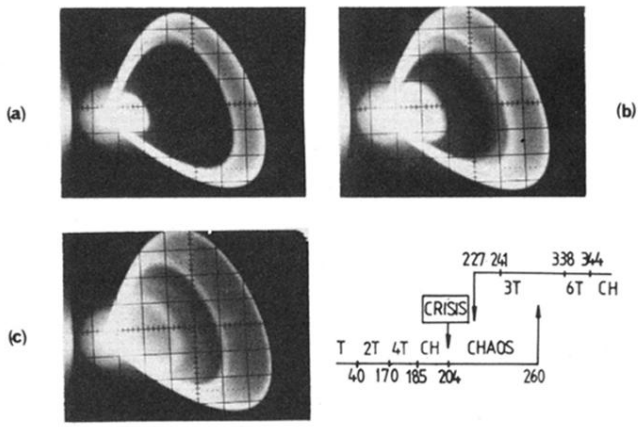

FIG. 17. $(I,\dot{I})$ plot in the crisis region at (a) 200 mV, (b) 204 mV, and (c) 208 mV driving voltages. The crisis is the same as that displayed in Fig. 16. (d) The situation of the crisis with respect to the "bistable" region is shown in the lower right part.

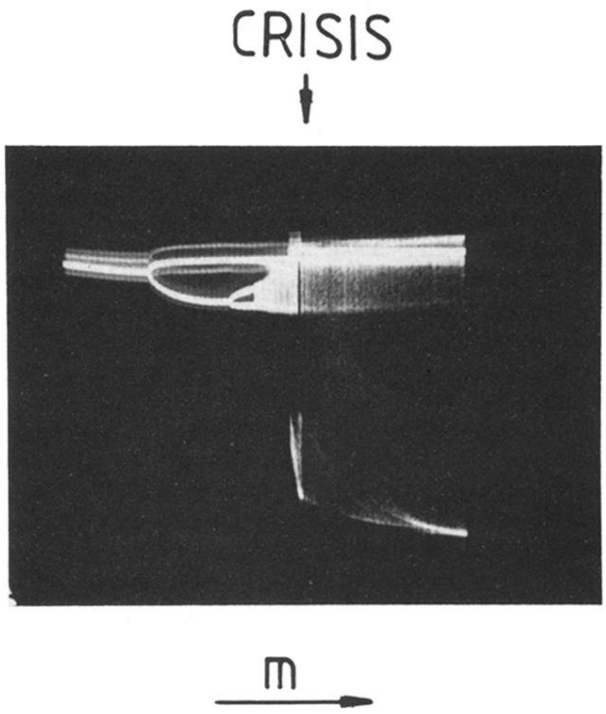

FIG. 19. Experimental BD in a large range of variation of the driving voltage. The crisis corresponds here to a sudden expansion of the chaotic attractor.

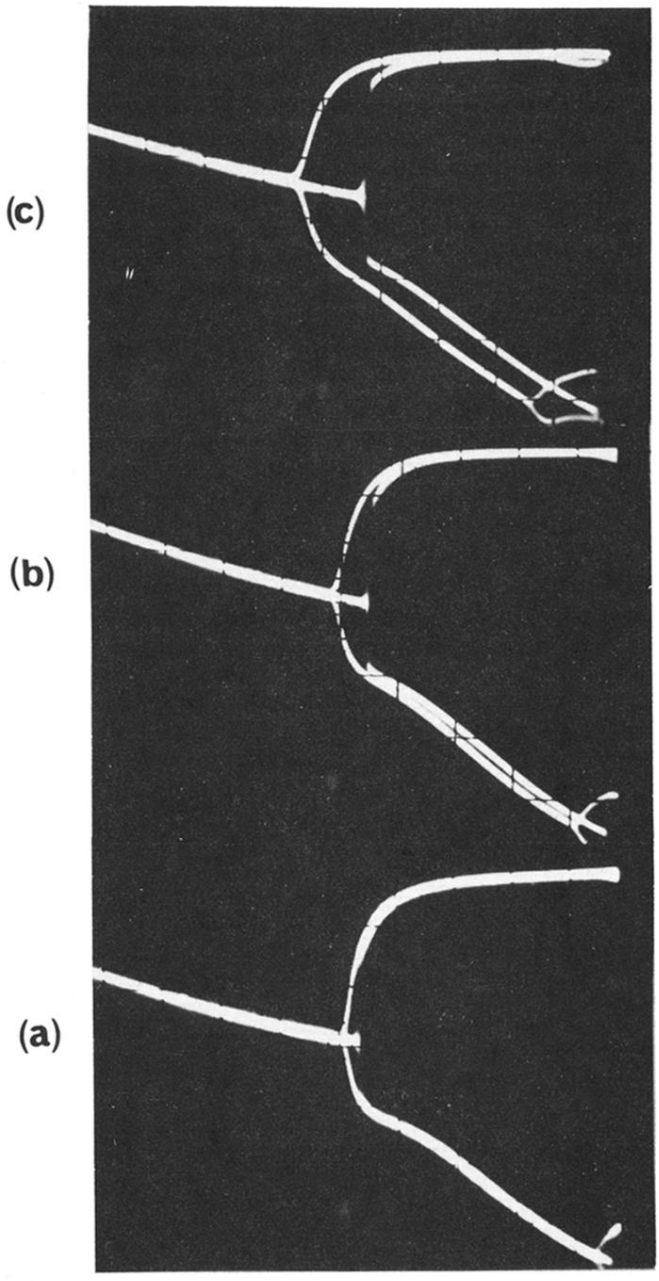

FIG. 20. Influence on the T-$2T$ bifurcation of the sweep frequency (a) 3 Hz, (b) 30 Hz, and (c) 300 Hz.

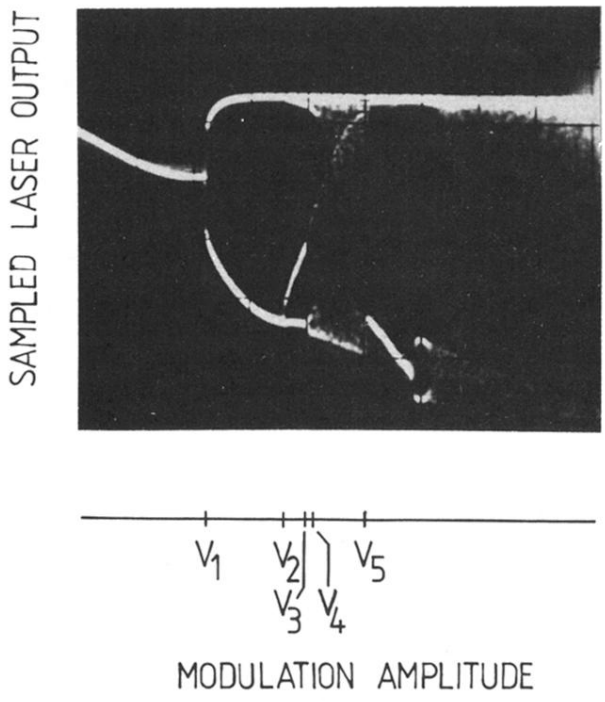

FIG. 7. Bifurcation diagram with the modulation amplitude as a control parameter.

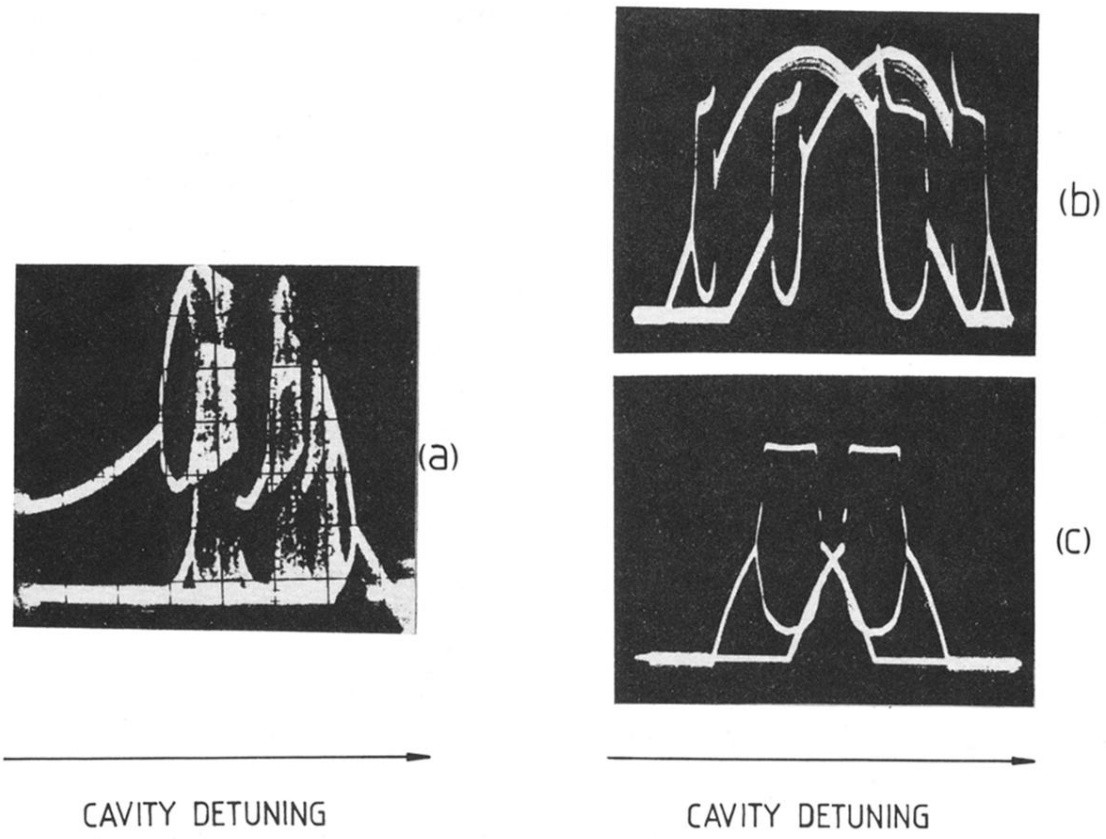

FIG. 8. Bifurcation diagrams obtained with the laser detuning as a control parameter for (a) high modulation amplitude and (b) and (c) low modulation amplitude. The most nonlinear regime has been obtained in the slope of the laser mode when the laser gain is low (c) and on top of the mode (zero detuning) when it is high (b). The detuning is swept over one mode width ($\sim$200 Mhz).

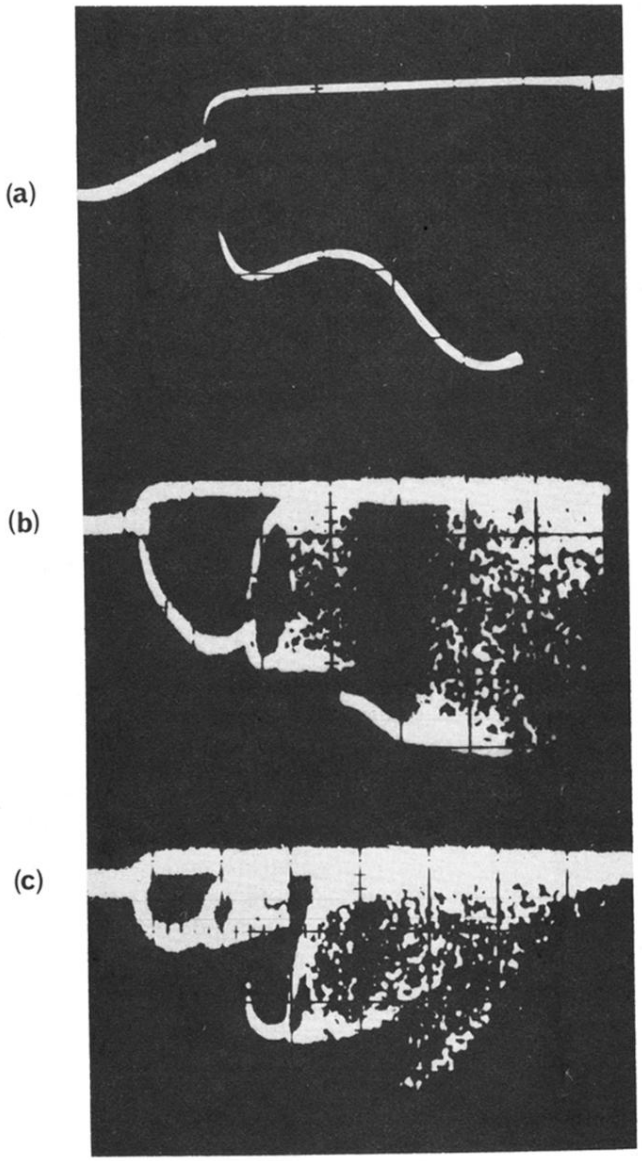

FIG. 9. Influence of the laser frequency on the BD obtained with the modulation amplitude as a control parameter in conditions of relatively low laser gain. The cavity detuning is, respectively, (a) 0, (b) 25, (c) 100 Mhz.